

RESEARCH

Open Access



# Thrombin-preconditioned mesenchymal stromal cell-derived extracellular vesicles attenuate experimental necrotizing enterocolitis

Sein Hwang<sup>1,2†</sup> , Se In Sung<sup>2,3†</sup>, Young Eun Kim<sup>2</sup>, Misun Yang<sup>2,3</sup>, Ara Koh<sup>4</sup>, So Yoon Ahn<sup>2,3</sup> and Yun Sil Chang<sup>1,2,3\*</sup> 

## Abstract

**Background** Necrotizing enterocolitis (NEC) is a critical gastrointestinal disease in preterm infants, for which no specific treatment is established. We previously demonstrated that thrombin-preconditioned mesenchymal stromal cell-derived extracellular vesicles (thMSC-EVs) enhance protection against other neonatal tissue injuries. Therefore, this study aimed to evaluate the therapeutic potential of thMSC-EVs in modified *in vitro*, *in vivo*, and organoid models of NEC.

**Methods** *In vitro*, the effects of thMSC-EVs and naïveMSC-EVs were compared in hyperosmotic, ischemic, and hypothermic (HIT)-stressed IEC-6 cells and LPS-treated peritoneal macrophages. *In vivo*, NEC was induced in P4 mouse pups by three cycles of formula feeding, oral LPS administration, hypoxia, and hypothermia, followed by overnight dam care.  $2 \times 10^9$  thMSC-EVs were intraperitoneally administered daily for three days, and the therapeutic effects were assessed macroscopically, histologically, and biochemically. NEC mouse-derived organoids were established to evaluate the thMSC-EVs' effect in mature enterocytes. LC-MS/MS was performed to analyze the EV proteomics.

**Results** *In vitro*, compared with naïveMSC-EVs, thMSC-EVs significantly improved cellular viability in HIT-induced IEC-6 cells and reduced pro-inflammatory (IL-1 $\alpha$ , IL-1 $\beta$ , TNF- $\alpha$ ) but increased anti-inflammatory (TGF- $\beta$ ) cytokine levels in LPS-treated peritoneal macrophages. *In vivo*, thMSC-EVs significantly attenuated clinical symptoms, reduced intestinal damage, and retained intestinal stem cell markers, showing more significant localization in NEC-induced intestines than in healthy intestines. In NEC mouse-derived organoids, thMSC-EVs significantly increased OLFM4 and claudin-4 expression and reduced stress-related markers such as sucrase-isomaltase, defensin, and chromogranin A. Proteomic analysis revealed that thMSC-EVs were greater enriched in anti-apoptotic, anti-inflammatory, cell adhesion, and Wnt signaling pathways than naïveMSC-EVs.

<sup>†</sup>Sein Hwang and Se In Sung contributed equally to this work.

\*Correspondence:  
Yun Sil Chang  
yschang@skku.edu

Full list of author information is available at the end of the article



© The Author(s) 2025. **Open Access** This article is licensed under a Creative Commons Attribution-NonCommercial-NoDerivatives 4.0 International License, which permits any non-commercial use, sharing, distribution and reproduction in any medium or format, as long as you give appropriate credit to the original author(s) and the source, provide a link to the Creative Commons licence, and indicate if you modified the licensed material. You do not have permission under this licence to share adapted material derived from this article or parts of it. The images or other third party material in this article are included in the article's Creative Commons licence, unless indicated otherwise in a credit line to the material. If material is not included in the article's Creative Commons licence and your intended use is not permitted by statutory regulation or exceeds the permitted use, you will need to obtain permission directly from the copyright holder. To view a copy of this licence, visit <http://creativecommons.org/licenses/by-nc-nd/4.0/>.

**Conclusion** thMSC-EVs improved cellular viability, reduced apoptosis, attenuated inflammation, and upregulated key intestinal stem cell markers, collectively suggesting their tissue-protective effects and highlighting their potential as a treatment for NEC.

**Keywords** Necrotizing enterocolitis, Mesenchymal stromal cells, Extracellular vesicles

## Background

Necrotizing enterocolitis (NEC) is a devastating neonatal gastrointestinal disease, particularly in very low birth weight infants, with an incidence of approximately 7% and an average mortality ranging from 20 to 30% [1–7]. NEC is a multifactorial disease of uncertain etiology associated with prematurity, enteral formula feeding, gut dysbiosis, infection, hypoxia, and hypothermia, contributing to the ambiguous nature of its pathophysiology [8, 9]. Despite advances in neonatal care, NEC remains a challenge with high mortality and morbidity, including the abrupt development of severe necrosis and inflammation, frequently requiring bowel resection, leading to short bowel syndrome and subsequent poor long-term neurodevelopment [10]. The persistent lack of NEC therapies adds to this challenge, and the development of NEC-targeted therapeutics is critical.

Multiple sources of stem cells, including MSCs, amniotic fluid stem cells, and placenta-derived stem cells, have been studied in NEC experimental models to develop novel NEC therapies [11–17]. The therapeutic effect of MSCs is mediated by extracellular vesicles encapsulating and delivering the MSCs' secretome to the injured area [18, 19], and several studies have investigated the therapeutic efficacy of MSC-derived extracellular vesicles (EVs) in NEC experimental models [20, 21]. We previously demonstrated that thrombin preconditioning prepares MSCs before transplantation by exposing them to a hemorrhagic injury-mimicking environment, ultimately enhancing their ability to secrete therapeutic cargo. Our previous study comparing different preconditioning methods with relevant neonatal injuries, such as hemorrhage, oxidative stress, and inflammation using thrombin, H<sub>2</sub>O<sub>2</sub>, and LPS, respectively, confirmed that thrombin was most effective in boosting EV biogenesis and angiogenic EV cargo enrichment via protease-activated receptor-mediated (PAR)-1 signaling pathways [19, 22]. Compared with naïve MSCs, thMSCs showed greater tissue-protective effects in animal models of hypoxic-ischemic encephalopathy and intraventricular hemorrhage (IVH), mediated by BDNF [23–25]. Subsequently, we confirmed the therapeutic efficacy of thMSC-EVs in other intractable disorders, such as neonatal meningitis and *E. coli*-induced acute lung injury animal models [26, 27].

Altogether with repeated confirmation of the anti-inflammatory, anti-apoptotic, and tissue-protective effects of thMSCs and thMSC-EVs in neonatal intractable

brain and lung disorders, this led us to explore whether these safer, cell-free EVs could offer similar benefits for NEC, a condition for which is characterized by severe acute inflammation, tissue injury, intestinal stem cells (ISCs) damage, and breached mucosal barrier and which no effective therapy has been established. Given the association of NEC pathophysiology with hemorrhage [28], we aimed to investigate the potential relevance of thMSC-EVs as a therapy. This study mimicked the pathophysiology of NEC using a newly established NEC in vitro model to compare the therapeutic efficacy of naïve MSC-EVs and thMSC-EVs, and analyzed their cargo proteomics. We further used the modified NEC in vivo model and its derived organoids to assess thMSC-EVs' therapeutic efficacy.

## Methods

### Ethics statements

Human WJ-MSCs from a single donor were provided by the Samsung Medical Center Good Manufacturing Practice Facility (IRB approval number: 2016-07-102-043). All animal studies were reviewed and approved by the Institutional Animal Care and Use Committee (approval numbers: 20231115001 and 20230116001) of Research Institute for Future Medicine (RIFM) of the Samsung Medical Center. RIFM is an Association for Assessment and Accreditation of Laboratory Animal Care International accredited facility and abide by the Institute of Laboratory Animal Resources guide. This study was conducted in accordance with the ARRIVE guidelines. Euthanasia followed the American Veterinary Medical Association (AMVA) Guidelines for the Euthanasia of Animals (2020).

### Thrombin-preconditioned Wharton's jelly (WJ)-MSC-derived EV production

WJ-MSCs at passage 7, which were cultured, expanded, and characterized according to the minimum criteria set by the International Society for Cell Therapy (Supplemental Fig. 1 A-B) were used for thrombin preconditioning and EV isolation, as previously described [27]. Briefly, WJ-MSCs were preconditioned with serum-free MEMα with or without 20 units/mL of thrombin (Reyon Pharmaceutical Co., Ltd., Seoul, South Korea) for 3 h [23]. The conditioned medium from naïve and thMSCs were diafiltered in Dulbecco phosphate buffered saline (DPBS) (Welgene, Daegu, South Korea) using a tangential flow filtration system (KrosFlo® KR2i, Repligen; Waltham,

MA, USA) with 300-kDa pore-sized mPES membrane to filter out debris and collect EVs. The quantity and surface markers of the isolated EVs were confirmed, as previously described (Supplemental Fig. 1C,D) [27]. Naïve and thMSC-EVs were diluted to a final concentration of  $2 \times 10^{10}$  EVs/mL and stored at  $-80^{\circ}\text{C}$  until use.

#### EV proteomic analysis

Liquid chromatography with tandem mass spectrometry (LC-MS/MS) analysis of isolated EVs was performed by ebiogen Inc. (Seoul, South Korea) to compare the proteomics of naïve MSC-EVs and thMSC-EVs. Isolated EVs underwent acetone precipitation, reduction, alkylation, and digestion before the analysis. Nano LC-MS/MS system (Nano-LC Ultimate 3000 & Thermo Orbitrap Exploris 480; Thermo Fisher Scientific, Waltham, MA, USA) was used. Data was analyzed using SAGE data dependent analysis and UniProt database. Data was interpreted using DAVID Bioinformatics (National Institutes of Health, Bethesda, MD, USA) Total of 1449 proteins were detected. Bubble plots were visualized using ExDEGA Graphic Plus software by ebiogen Inc. The detailed method can be found in the Supplementary Material 1.

#### Multiple-hit in vitro model

IEC-6 cells were obtained from ATCC and maintained in Dulbecco's Modified Eagle Medium (DMEM) supplemented with 10% FBS and 1% penicillin/streptomycin in a 5%  $\text{CO}_2$  humidified chamber. In all in vitro experiments, IEC-6 cells ( $2 \times 10^5$  cells/mL) were seeded in 96-, 24-, and 12-well cell culture plates (Thermo Fisher Scientific, Waltham, MA, USA) and stabilized for 24 h. Naïve and thMSC-EVs were 1:10 diluted in the culture media to a final concentration of  $2 \times 10^9$  EVs/mL for treatment.

Induction of hyperosmotic, ischemic, and hypothermic stress (HIT) was performed by replacing the media with 1% v/v dextran sodium sulfate (DSS) supplemented with serum and glucose-free DMEM incubated in 1%  $\text{O}_2$  chamber at  $32^{\circ}\text{C}$  for 24 h. DSS is a 40-kDa molecule commonly used in inflammatory bowel disease (IBD) models to induce hyperosmotic stress [29–31]. After 24 h, the media were replaced with serum-free DMEM treated with 1:10 diluted DPBS (HIT group), naïveMSC-EVs (HIT + naïveEV), or thMSC-EVs (HIT + thEV group).

#### Inflammatory in vitro model

Primary rat peritoneal macrophages (PMs) were collected from P11 Sprague-Dawley rats. Rats were euthanized using a lethal dose of isoflurane in a closed chamber. After sacrifice, 3 mL of DMEM was intraperitoneally injected and collected using a 3-mL syringe. The collected peritoneal fluid was centrifuged at  $500 \times g$  for 10 min and cultured in 6-well plates (Thermo Fisher Scientific). After 24 h of stabilization, media were replaced with  $0.1 \mu\text{g}/$

mL LPS (O111:B4; Sigma Aldrich; Burlington, MA, USA) in serum-free DMEM with a 1:10 volume dilution of PBS (LPS group), naïveMSC-EVs (LPS + naïveEV group), or thMSC-EVs (LPS + thEV group). Cells were incubated in 1%  $\text{O}_2$  hypoxic chamber for 24 h, and the CM was collected. The IEC-6 cells were treated with the collected CM for 24 h (LPS CM, LPS + naïveEV CM, and LPS + thEV groups). Inflammatory cytokine levels in the CM were also measured using ELISA.

#### Cell viability

Cell viability was measured using CCK-8 assay (Dojindo laboratory; Kumamoto, Japan). 1:10 CCK-8 reagent diluted to serum-free DMEM media were treated to IEC-6, incubated for 10 min, and measured at 450 nm using a microplate reader.

#### NEC mouse model

The work has been reported in line with the ARRIVE guidelines 2.0 and the inclusion and exclusion criteria were established a priori. The NEC induction protocol was modified based on several animal models and prepared before the study [32–34]. Postnatal day 4 (P4) outbred ICR strain mouse pups weighing 2.5–3 g were used. ICR mice show high genetic variance and reproduction rate, yielding about 11 pups. The mice were randomly divided into the following experimental groups: normal control (CON), NEC control (NEC), and NEC treated with EVs (NEC + thEV). In each experimental set, 4, 10, and 10 pups were allocated to CON, NEC, and NEC + thEV groups, respectively, considering that 14 litters per surrogate mother are provided by the laboratory animal supplier and considering the primary outcome established a priori. Any mouse pup that lost significant weight was considered for humane endpoint, but none was observed. Every morning at 9 am, mouse pups were separated from the dam, and their body weights were measured. In total,  $60 \mu\text{g}$  LPS ( $6 \mu\text{L}$  of  $10 \mu\text{g}/\mu\text{L}$  LPS) was orally administrated to mouse pups using a  $10\text{-}\mu\text{L}$  pipette. The hyperosmolar formula was prepared by adding the powdered formula (7.5 g) (Maeil, Seoul, South Korea) to 30 mL of Esbilac liquid puppy replacement milk (Pet Ag, Hampshire, Illinois, USA).  $100 \mu\text{L}/3 \text{ g}$  body weight of hyperosmolar formula was gavage-fed to mouse pups using a 22-gauge (G) feeding tube (FTP 22–25; Instech Laboratories Inc., Plymouth Meeting, PA, USA) and a 1-French G polyurethane catheter (HC-SP130; Insung Medical; Gangwon-do, South Korea). Hypothermia was induced in the fed mice by exposure to  $4^{\circ}\text{C}$  for 10 min, followed by hypoxia induction by exposure to 5%  $\text{O}_2$  95%  $\text{N}_2$  gas in the chamber for 20 min. Next,  $100 \mu\text{L}$  of PBS or  $2 \times 10^{10} / \text{mL}$  thMSC-EVs were intraperitoneally (IP) administered at 9 am for three consecutive days immediately after hypoxia exposure, using a 1-mL insulin syringe

(6-mm needle; 320320; BD Bioscience, Franklin Lakes, NJ, USA). The dosage was referenced from other studies that treated  $2.5 \times 10^9$  EVs per NEC-induced animal [20, 21]. Three cycles of gavage feed, hypoxia, and hypothermia induction were performed every 4 h daily. Mouse pups were placed in 36 °C incubator in between cycles for body temperature stabilization without the dam. At 6 pm, immediately after the final induction, mouse pups were returned to their cages with a dam together with CON pups overnight. At P7, for tissue collection, mouse pups were euthanized in a closed chamber using a lethal dose of isoflurane (Hana Pharm Co., LTD; Seoul, South Korea). Dams were euthanized using a CO<sub>2</sub> euthanasia chamber, followed by a cervical dislocation. Body weight and survival were assessed daily, and only those that survived the completion of the study were included in the analysis. The protocol was performed in the same order and at similar times to minimize potential confounders. The primary outcome measure in determining the sample size was histological damage score.

#### Clinical sickness score

The clinical sickness score was measured in each pup at P7, immediately before sacrifice, by a single investigator blinded to the experimental group. The scoring rubric developed by Zani et al. was modified for this study [33] (Table 1)

#### In vivo and ex vivo near-infrared fluorescence (NIRF) optical imaging

The thMSC-EVs were tagged with green fluorescent PKH67 (Sigma Aldrich) or subjected to NIRF optical imaging. At room temperature, 6 µg of PKH67 was incubated with 1 mL of thMSC-EVs for 5 min. The thMSC-EVs were washed and ultracentrifuged to collect

thMSC-EVs and remove free dyes. In healthy CON mice, optical NIRF imaging was conducted at 3 and 24 h after the administration of PKH-tagged thMSC-EVs. To compare the distribution of thMSC-EVs between CON and NEC groups, PKH-tagged thMSC-EVs were administered using an in vivo protocol. Optical NIRF imaging was conducted at P7. Details of the imaging procedure are specified in the Supplementary Material 1.

#### Tissue preparation for histological analysis

Immediately after sacrifice, the ileum was swiss-rolled into a cassette, fixed with 4% paraformaldehyde, and embedded in a paraffin block so that the slides could be longitudinally sectioned. Embedded tissues were sectioned into 4-µm thick slides. The cross-sectional slide that showed the intestinal wall and villi longitudinally was selected for hematoxylin and eosin and immunofluorescence staining. For all histological analyses, a single investigator who was blinded to the experimental group scored the six images taken from each histological slide.

#### Histological damage score measurement

Images taken under 20× magnification using a light microscope were used. The histological damage score was measured using the following criteria: grade 0, intact villi and eosinophilic cytoplasm; grade 1, intact villi and pale cytoplasm; grade 2, loss of villi and pale cytoplasm; and grade 3, severe sloughing of villi resulting in areas without villi. An established score rubric [33] was modified for this study, and a single investigator who was blinded to the experimental group measured the histological damage score.

#### Establishment of the NEC mouse-derived organoids

The organoids were independently established from six NEC-induced mice following the established protocol (Supplementary Material 1) [35]. Each mouse organoid was differentiated and supplemented with PBS (NEC) or thMSC-EVs (NEC + thEV). Basal media containing EGF, noggin, and R-spondin (ENR medium) supplemented with a 1:10 dilution of PBS or thMSC-EVs were replaced every 48 h for 7 days. On day 7, organoids were collected for RNA isolation. Differentiation was confirmed through immunofluorescent staining of E-cadherin, MUC2, OLFM4, villin, and chromogranin A and by quantification of budded organoids.

#### TUNEL assay

To analyze dead cells, TdT-mediated dUTP Nick-End Labeling (TUNEL) assay was performed using the Dead-End™ Fluorometric TUNEL System (Promega, Madison, WI, USA), according to the manufacturer's instructions.

**Table 1** Rubric for the clinical sickness score

| Clinical Sickness Score Rubric |                                    |                          |                                    |   |                  |
|--------------------------------|------------------------------------|--------------------------|------------------------------------|---|------------------|
| Score                          | Appearance                         | Respiration              | Response to Touch                  | Natural Activity                          | Body Color       |
| 0                              | Tonic & well hydrated              | Normal                   | Alert without stimulation          | Normal                                    | Pink             |
| 1                              | Slimmer but still tonic & hydrated | Gasping                  | Responding to mild stimulation     | Able to strongly wriggle if placed supine | Pale extremities |
| 2                              | Skinny, floppy, & dehydrated       | Visible chest retraction | Responding to vigorous stimulation | Able to weakly wriggle if placed supine   | Pale body        |
| 3                              | Gasping & in agony                 | Unable to breathe        | Unresponsive                       | Not moving & lying still                  | Gray             |

## ELISA

For mouse intestinal cytokine measurements, the collected ileum was homogenized in PBS supplemented with a protease inhibitor (Invitrogen, Carlsbad, CA, USA) using a homogenizer (DWK Life Sciences, Wertheim, Germany). Cell culture media were used for the *in vitro* cytokine measurements, and the 5-plex Rat Luminex Discovery assay and 5-plex Mouse Luminex Discovery assay, each including interleukin (IL)-1 $\alpha$ , IL-1 $\beta$ , IL-6, tumor necrosis factor (TNF)- $\alpha$ , and transforming growth factor (TGF)- $\beta$  (R&D Systems, Minneapolis, MN, USA), were used following the manufacturer's instructions.

## Immunofluorescent staining

The tissue slides were deparaffinized and boiled for 20 min in Tris-EDTA buffer (Biosesang, Gyeonggi-do, South Korea) for antigen retrieval. Cell cultures fixed in 4% paraformaldehyde were permeabilized in 0.1% Triton-100 supplemented with PBS. Primary antibodies were incubated overnight at 4 °C, washed, incubated with secondary antibodies for 2 h at room temperature, and counterstained with DAPI. Tissue slides were mounted with a fluorescence mounting medium (DAKO, Santa Clara, CA, USA) and stored at 4 °C. The following primary antibodies were used: E-cadherin (1:1000; BD Bioscience), MUC2 (1:1000; Abcam, Cambridge, UK), chromogranin A (CHGA) (1:500; ImmunoStar, Hudson, WI, USA), lysozyme (1:1000; Abcam), and OLFM4 (1:1000; Cell Signaling, Danvers, MA, USA).

Organoids were stained using the protocol "Performing Immunocytochemical Staining of Epithelial Organoids" provided by STEMCELL Technologies (Vancouver, BC, Canada). Primary antibodies were diluted 1:100 for organoid staining.

## Cell quantification

All images were captured under the same confocal microscope settings and analyzed by a blinded single investigator. Six random areas were analyzed per sample. The counted cell numbers in the histological slides were normalized to the intact villi represented by the DAPI intensity. Cultured cells were normalized to the total number of cells, which was calculated using ImageJ software (National Institutes of Health, Bethesda, MD, USA). The numbers of MUC2- and TUNEL-positive cells were automatically calculated using ImageJ software using threshold, binary, watershed, and measurement functions.

## Western blot analysis

Cells were removed from the medium, washed, replaced with RIPA buffer (Biosesang) supplemented with a protease inhibitor (Invitrogen), scraped using a cell scraper (SPL, Gyeonggi-do, South Korea), and collected in 1.5-mL tubes. The cells were sonicated and centrifuged at full

speed for 15 min at 4 °C. Protein extracts were quantified using a BSA protein assay kit (Thermo Fisher Scientific). The proteins were diluted to a final concentration of 200  $\mu$ g/mL. SDS-PAGE gel electrophoresis was performed. Bolt Tris-Bis plus mini 6% polyacrylamide gels (Invitrogen) were used for ZO-1 detection and 4–12% gels (Invitrogen) were used for GAPDH detection. The gels were transferred at 100 V for 1 h 30 min. Nitrocellulose membranes were blocked in 5% skim milk PBS + 0.1% Tween 20 (PBST) at room temperature for 1 h. Primary antibodies of ZO-1 (1:1000, 40-2200; Invitrogen) and GAPDH (1:1000; Santa Cruz, Dallas, TX, USA) were placed in 5% skim milk PBST overnight at 4 °C, washed, incubated with secondary antibodies for 1 h, and washed. Amersham ECL detection reagents (Cytvia, Marlborough, MA, USA) were used to detect protein under the Amersham AI600 chemiluminescent imager (Cytvia). ImageJ software was used to measure the band intensity. Whole blot images can be found in the Supplementary Fig. 6.

## RT-qPCR

After sacrifice, the ileum was collected and stored in an RNaprotect reagent (Qiagen, Germantown, MD, USA) at -80 °C. For mRNA extraction, the Xenopure total RNA purification kit (Xenohelix; Incheon, South Korea) was used as per the manufacturer's protocol. cDNA was synthesized using the Primescript RT reagent kit (Takara, Shiga, Japan), quantified, diluted to 100 ng/ $\mu$ L, and amplified using AccuPower 2X Greenstar qPCR master mix (Bioneer, Daejeon, South Korea) and the Quantstudio 6 Flex system (Thermo Fisher Scientific). The list and sequences of primers are provided in the Supplementary Material 1.

## Statistical analysis

One-way analysis of variance, post-hoc Tukey test, and Bonferroni correction, as necessary, were used to compare data between the experimental groups. The normal distribution was confirmed before performing the Tukey test and Bonferroni correction. Bar graphs present the data as mean  $\pm$  standard error of the mean and dots of individual values. The nonparametric Mann-Whitney U test was used to analyze the RT-qPCR data. GraphPad Prism 8.0 software (GraphPad, San Diego, CA, USA) was used to perform data analysis, and a *p*-value < 0.05 was considered statistically significant. Fisher's exact statistic was used in the DAVID bioinformatics to analyze protein enrichment. Adjusted *p*-value < 0.05 was considered statistically significant.

**Result**  
**thMSC-EVs significantly enhanced cellular viability and integrity upon hyperosmotic, ischemic, and hypothermic stress to IEC-6 cells**

To mimic the multifactorial nature of NEC pathophysiology, we induced HIT in IEC-6 cells (Fig. 1A). In the CCK-8 assay, the percentage of viable IEC-6 cells was significantly reduced in the HIT group than in the CON group. Compared with the HIT group, the HIT + naïveEV and HIT + thEV groups showed a significant increase in cell viability; however, the effect was significantly greater in the in HIT-thEV group than in the HIT + naïveEV group. According to the TUNEL assay, the HIT and HIT + naïveEV groups had significantly higher TUNEL-positive cell counts than did the CON group; however, the HIT + thEV group was not statistically different from the CON group. The level of ZO-1, marker of cellular integrity, was significantly lower in the HIT group than in the CON group. The reduction in ZO-1 levels in the HIT group was significantly restored in the HIT + thEV group but not in the HIT + naïveEV group. Overall, thMSC-EVs

showed greater effects in enhancing cellular viability and integrity than did naïveMSC-EVs in HIT-induced IEC-6 cells.

**thMSC-EVs significantly reduced pro-inflammatory cytokines in LPS-induced PMs**

The CM was treated to IEC-6 cells for cellular viability assessment, and inflammatory cytokine levels were measured using ELISA. Compared with the CON group, LPS CM treatment significantly decreased IEC-6 cell viability (Fig. 1B). This decrease was significantly restored by treatment with LPS + thEV CM but not with LPS + naïveEV CM. Levels of pro-inflammatory cytokines IL-1 $\alpha$ , IL-6, IL-1 $\beta$ , and TNF- $\alpha$  and anti-inflammatory cytokine TGF- $\beta$  were also measured in the same CM (Fig. 1C). Compared with the CON group, the LPS group showed significantly greater levels of all pro-inflammatory cytokines. The elevated cytokine levels were significantly reduced in the LPS + thEV group, and this anti-inflammatory effect was notably more pronounced than that in the LPS + naïveEV group. Anti-inflammatory

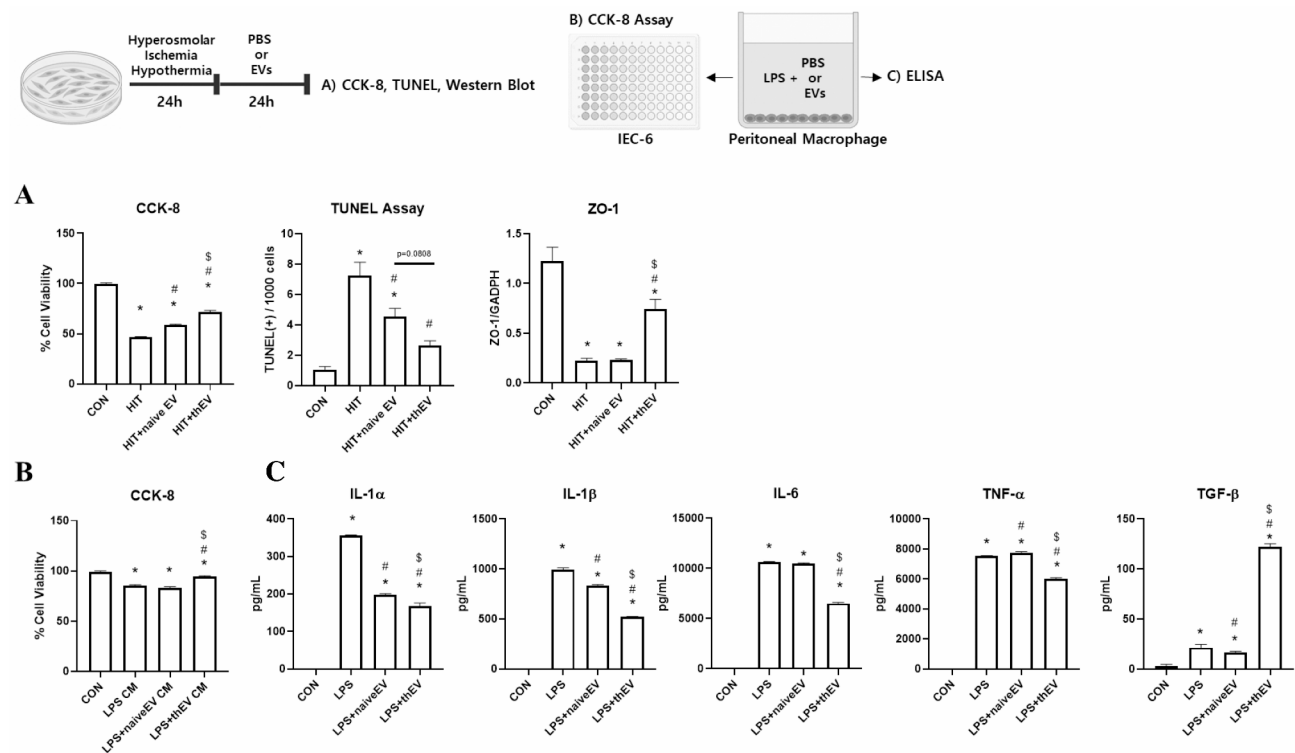


**Fig. 1** thMSC-EVs significantly improved cell viability, cell integrity, and inflammation in NEC in vitro models. **(A)** Bar graph representation of CCK-8 cell viability assay, TUNEL assay, and western blot protein expression levels of ZO-1 in IEC-6 cells.  $n = 16, 16, 16,$  and  $16$  for the CCK-8 assay;  $n = 10, 10, 10,$  and  $10$  for the TUNEL assay; and  $n = 3, 3, 3,$  and  $3$  for western blot analysis in the CON, HIT, HIT + naïveEV, and HIT + thEV groups, respectively. \*,  $p < 0.01$  vs. CON; #,  $p < 0.01$  vs. HIT; \$,  $p < 0.01$  vs. HIT + naïveEV. **(B)** Bar graph representation of CCK-8 cell viability assay in LPS-induced peritoneal macrophage CM-treated IEC-6 cells.  $n = 16, 16, 16,$  and  $16$  in the CON, LPS CM, LPS + naïveEV CM, and LPS + thEV CM groups, respectively. **(C)** Bar graph showing inflammatory cytokine levels in LPS-induced peritoneal macrophages.  $n = 4, 4, 4,$  and  $4$  in the CON, LPS, LPS + naïveEV, and LPS + thEV groups, respectively. \*,  $p < 0.01$  vs. CON; #,  $p < 0.01$  vs. LPS; \$,  $p < 0.01$  vs. LPS + naïveEV. Data are presented as mean  $\pm$  SEM. One-way ANOVA and the post-hoc Tukey test were used in the analysis. CON, normal control; HIT, hyperosmolar stress, ischemia, and hypothermia-induced IEC-6 cells; LPS, lipopolysaccharide; naïve MSC-EVs, naïve MSC-derived EVs; thMSC-EVs, thrombin-preconditioned MSC-derived EVs

cytokine TGF- $\beta$  levels were significantly increased in the LPS + thEV group than in the LPS group and distinctively greater than those in the LPS + naïveEV group.

### Intraperitoneal administration of thMSC-EVs significantly improved the clinical symptoms in NEC-induced mouse pups

Smaller body size and enlarged gastrointestinal (GI) sizes confirmed successful NEC induction in neonatal mouse pups, despite overnight breastfeeding, demonstrating the validity and feasibility of our protocol (Supplemental Fig. 2A). At P7, the body weights were significantly lower in the NEC and NEC + thEV groups than in the CON group, with no significant difference between the NEC and NEC + thEV groups (Fig. 2A). The survival rates were 100%, 58.11%, and 65.28% in the CON, NEC, and NEC + thEV groups, respectively (Fig. 2A). The survival rates were significantly lower in the NEC and NEC + thEV groups than in the CON group, with no significant difference between the NEC and NEC + thEV groups. At P7, the clinical sickness scores were significantly higher in all NEC-induced groups than in the CON group; however, daily IP administration of thMSC-EVs significantly reduced the clinical sickness scores in the NEC + thEV group (Fig. 2B). The GI length from the stomach to the rectum was significantly shorter in the NEC group than in the CON group (Fig. 2C), with no significant difference between CON and NEC + thEV.

### Intraperitoneal administration of thMSC-EVs distributed greater to the NEC-induced Gastrointestinal tract than to the healthy tract

To validate that IP administration effectively targets the GI tract, uptake of PKH-tagged thMSC-EVs was first evaluated in healthy mouse pups (Supplemental Fig. 3A). The NIRF imaging demonstrated a trend in which thMSC-EVs remain within the peritoneum by 3 h but measurably diffuse into the small intestine by 24 h. The

differential fluorescent intensity between CON and NEC group at P7 confirmed a significantly greater thMSC-EVs distribution in the injured NEC GI tract than in the healthy GI tract (Supplemental Fig. 3B).

### Intraperitoneal administration of thMSC-EVs significantly attenuated the histological damage in NEC-induced mouse pups

Histological assessment confirmed successful NEC induction despite overnight breastfeeding. One of the key histological differences between the CON and NEC groups was the appearance of cell swelling and necrotic cells, featuring pale cytoplasm or “ghost-like” crypt-villus histoarchitecture [36, 37] (Fig. 3A). The disrupted epithelial integrity was further visualized via E-cadherin staining, which revealed an irregular cell membrane lining (Fig. 3C). The histological damage score representing villus loss severity was significantly higher in all NEC-induced groups than in the CON group, and it was significantly higher than that in the NEC + thEV group (Fig. 3B).

Quantified MUC2-positive goblet cells, normalized by DAPI intensity to account for villus depletion, were significantly reduced in the NEC group compared with those in the CON group, and were significantly restored in the NEC + thEV group (Fig. 3D).

### Intraperitoneal administration of thMSC-EVs significantly increased intestinal stem cell (ISC) marker gene expression in NEC-induced mouse pups

The expression of ISC marker genes olfactomedin 4 (OLFM4), leucine-rich repeat-containing G-protein coupled receptor 5 (LGR5), and the secretory cell differentiation gene atonal BHLH transcription factor 1 (ATOH1) were analyzed using RT-qPCR (Fig. 4A). The expression levels of OLFM4 and LGR5 were significantly reduced in the NEC group compared with those in the CON group and were significantly increased in the NEC + thEV

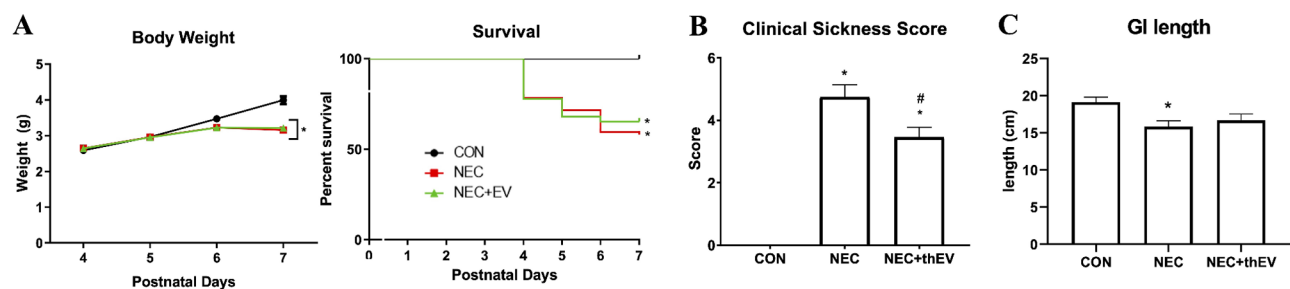


**Fig. 2** Intraperitoneal administration of thMSC-EVs improved the clinical symptoms in NEC-induced mouse pups. (A) Graphical representations of daily body weight measurements and percent survival of mouse pups.  $n = 23, 40, 43$  in the CON, NEC, and NEC + thEV groups, respectively. (B) Bar graph representation of clinical sickness score assessment at P7.  $n = 8, 16, 13$  in the CON, NEC, and NEC + EV groups, respectively. (C) Bar graph representation of GI length measured at P7.  $n = 8, 16, 13$  in the CON, NEC, and NEC + thEV groups, respectively. Data are presented as mean  $\pm$  SEM. \*,  $p < 0.01$  vs. CON; #,  $p < 0.01$  vs. NEC. The log-rank test was used to compare the survival rate between the groups. One-way ANOVA and the post-hoc Tukey test were used in all other analyses. CON, normal control; NEC, necrotizing enterocolitis control group; NEC + thEV, thMSC-EVs treated NEC group

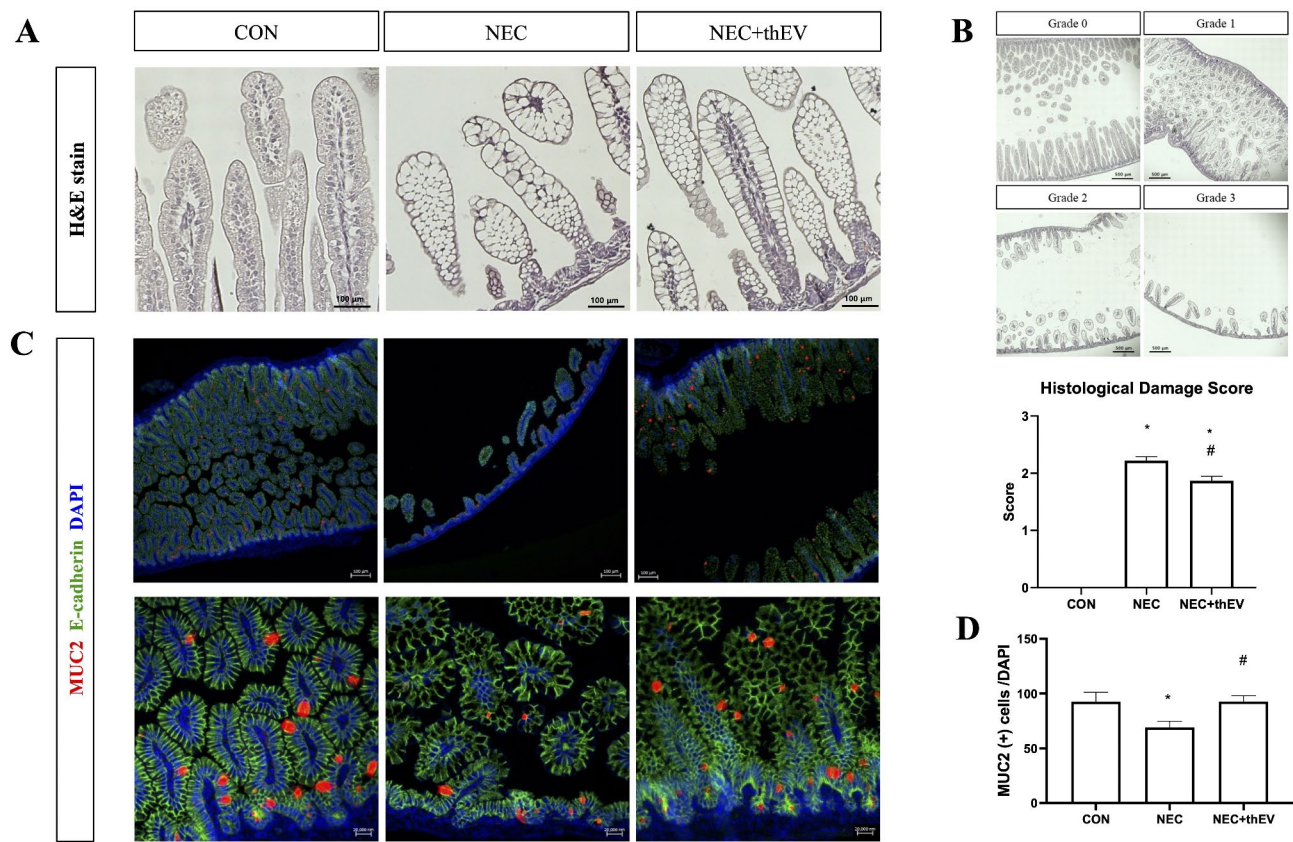


**Fig. 3** Intraperitoneal administration of thMSC-EVs attenuated the histological damage in NEC-induced mouse pups. **(A)** Representative microscopic images of H&E-stained histology slides. **(B)** Bar graph representation of histological damage score assessment.  $n=11, 21,$  and  $25$  in the CON, NEC, and NEC+thEV groups, respectively. **(C)** Representative microscopic images of immunofluorescent staining. **(D)** Bar graph representation of quantification of MUC2 (+) cells.  $n=6, 7,$  and  $11$  in the CON, NEC, and NEC+EV groups, respectively. Data are presented as mean  $\pm$  SEM. \*,  $p < 0.01$  vs. CON; #,  $p < 0.01$  vs. NEC. One-way ANOVA and the post-hoc Bonferroni test were used in the analysis. CON, normal control; NEC, necrotizing enterocolitis control group; NEC+thEV, thMSC-EVs treated NEC group

group. ATOH1 expression was significantly reduced in the NEC and NEC+thEV groups compared with that in the CON group, although the difference between the NEC and NEC+thEV groups did not reach statistical significance. The mean fold-change values for ATOH1 were 0.4161 and 0.7022, respectively, indicating an increasing trend.

#### Intraperitoneal administration of thMSC-EVs significantly reduced cell death in the intestinal crypt in NEC-induced mouse pups

All NEC-induced groups showed a significantly greater number of TUNEL-positive cells than that in the CON group, with the NEC+thEV group showing significantly fewer TUNEL-positive cells than those in the NEC group (Fig. 4B). TUNEL-positive cells were predominantly localized near the crypt base, where ISCs reside, as confirmed by the TUNEL assay and OLFM4 staining (Fig. 4D and E).

Fatty acid-binding protein (FABP) expression, which is associated with intestinal injuries, including NEC

[38–41], was significantly greater in the NEC and NEC+thEV groups than in the CON group, and the NEC+thEV group exhibited significantly lower levels than did the NEC group (Fig. 4A). Specifically, the NEC group showed an approximately 70-fold increase in FABP6 expression, whereas the NEC+thEV group showed an approximately 30-fold reduction.

#### thMSC-EVs significantly reduced pro-inflammatory cytokine IL-1 $\alpha$ levels in NEC-induced mouse pups

Pro-inflammatory cytokine IL-1 $\alpha$  level was significantly increased in the NEC and NEC+thEV groups compared with that in the CON group (Fig. 4C). However, compared with the NEC group, the NEC+thEV group showed significantly reduced levels.

#### thMSC-EVs significantly enhanced the expression of OLFM4 and Claudin and reduced the expression of defensin and CHGA in NEC organoids

Organoids were differentiated for 7 days with or without thMSC-EV treatment. On day 7, organoids were

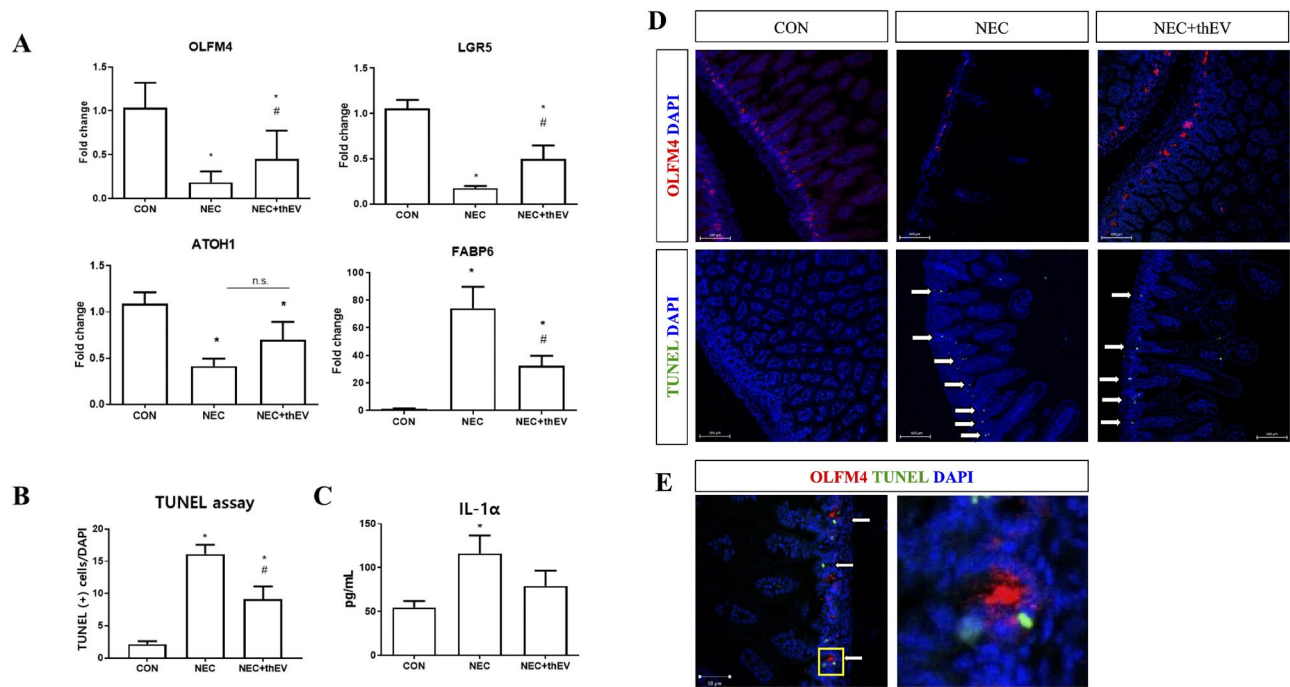


**Fig. 4** Intraperitoneal administration of thMSC-EVs increased goblet cells and ISC marker gene expression in NEC-induced mouse pups. **(A)** Bar graph representation of the expression levels of intestinal marker genes *LGR5*, *OLFM4*, *ATOH1*, and *FABP6* analyzed via RT-qPCR.  $n = 16, 11,$  and  $16$  in the CON, NEC, and NEC + thEV groups, respectively. The Mann–Whitney test was used for the analysis. **(B)** Bar graph representation of the count of TUNEL (+) cells.  $n = 11, 21,$  and  $25$  in the CON, NEC, and NEC + thEV groups, respectively. One-way ANOVA and the post-hoc Bonferroni test were used in the analysis. **(C)** Bar graph representation of pro-inflammatory cytokine IL-1 $\alpha$  levels measured using ELISA.  $n = 18, 23,$  and  $19$  in the CON, NEC, and NEC + EV groups, respectively. **(D)** Representative microscopic image of immunofluorescent-stained OLFM4 (+) cells and TUNEL (+) cells. **(E)** Representative microscopic image of merged OLFM4 and TUNEL (+) cells. One-way ANOVA and the post-hoc Bonferroni test were used in the analysis. White arrows point to TUNEL (+) cells. Data are presented as mean  $\pm$  SEM. \*,  $p < 0.01$  vs. CON; #,  $p < 0.01$  vs. NEC. CON, normal control; NEC, necrotizing enterocolitis control group; NEC + thEV, thMSC-EVs treated NEC group

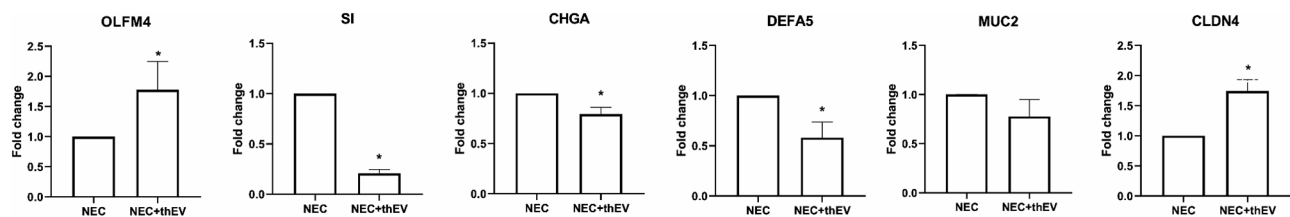


**Fig. 5** thMSC-EVs' effect in gene expression levels of differentiated NEC organoids. Bar graph representation of intestinal organoid marker gene expression levels analyzed using RT-qPCR.  $n = 4$  and  $4$  in the NEC and NEC + thEV groups, respectively. Data are presented as mean  $\pm$  SEM. \*,  $p < 0.01$  vs. NEC. The Mann–Whitney test was used in the analysis. CON, normal control; NEC, necrotizing enterocolitis control group; NEC + thEV, thMSC-EVs treated NEC group

collected, and differentiation was confirmed through immunofluorescent staining (Supplemental Fig. 5A). The extent of differentiation was analyzed by counting cystic and budded organoids (Supplemental Fig. 5B). The mean  $\pm$  SEM percent of budded organoids in the CON and CON+thEV groups were  $50.1 \pm 5.2$  and  $62.7 \pm 8.8$ , respectively, and those in the NEC and NEC+thEV groups were  $56.5 \pm 5.2$  and  $63.6 \pm 2.5$ , respectively. Treatment of thMSC-EVs showed an increasing trend in the percentage of budded organoids without statistical significance.

On day 7, the organoids were collected for mRNA isolation via RT-qPCR. The differential gene expression

levels of *OLFM4* (ISC marker), sucrase-isomaltase (*SI*, absorptive enterocyte marker), chromogranin A (*CHGA*, enteroendocrine cell marker), defensin (*DEFA5*, Paneth cell marker), mucin (*MUC2*, goblet cell marker), and claudin-4 (*CLDN4*, tight junction marker) in the organoids were analyzed (Fig. 5). The comparison between the CON and NEC organoids was confirmed first (Supplemental Fig. 5C). NEC organoids were treated with or without thMSC-EVs and analyzed.

In NEC + thEV organoids, *OLFM4* and *CLDN4* expression levels were significantly higher than those in NEC organoids, indicative of adult ISCs and cellular integrity. Conversely, the expression levels of *SI*, *CHGA*, and

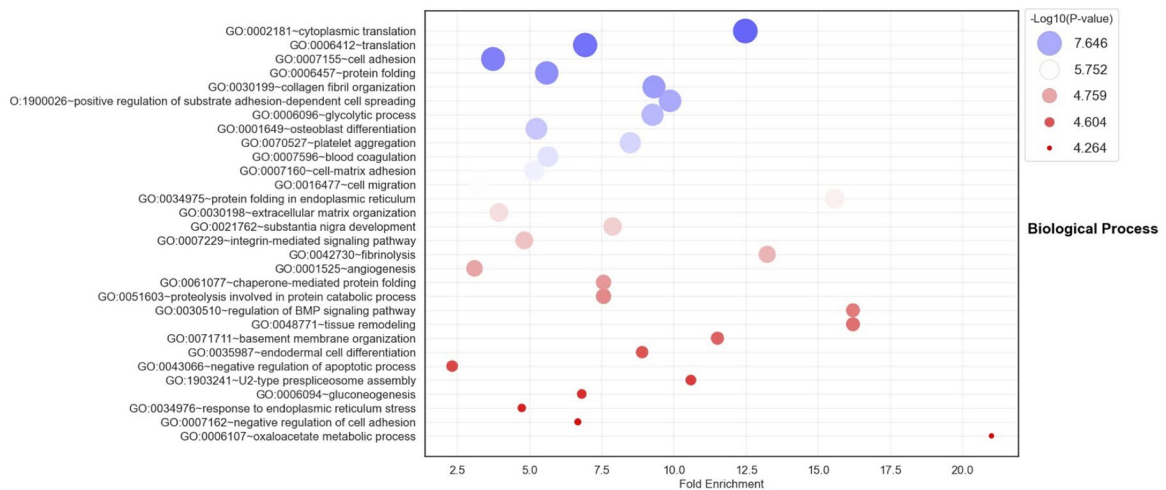
*DEFA5* were significantly reduced in NEC + thEV organoids compared with those in NEC organoids. *MUC2* expression was approximately five-fold higher in NEC organoids than in CON organoids, and NEC organoids treated with thMSC-EVs showed a 0.7-fold reduction in *MUC2* expression, although this difference was not statistically significant.

**thMSC-EVs are enriched in anti-apoptotic, anti-inflammatory, cell adhesion, and Wnt signaling pathways compared to the naïveMSC-EVs**

EVs isolated using the TFF system diafiltrated with DPBS minimized the potential inclusion of proteins outside of

the EVs in the proteomic analysis. A list of proteins that had an abundance value greater than two-fold present in the thMSC-EVs compared with the naïveMSC-EVs were exported and analyzed using the DAVID bioinformatics Gene Ontology Biological Processes database. The top 30 biological pathways (BP) enriched in thMSC-EVs compared to naïveMSC-EVs were pathways of cellular metabolism, angiogenesis, blood coagulation, integrin-mediated signaling, protein folding, basement membrane organization, and anti-apoptosis (Fig. 6A). To understand the in vitro, in vivo, and organoid results, the anti-apoptosis, anti-inflammation, cell-cell adhesion, and Wnt signaling pathways were selectively examined (Fig. 6B).

**A** Top 30 Biological Processes



**B** Selected Biological Processes

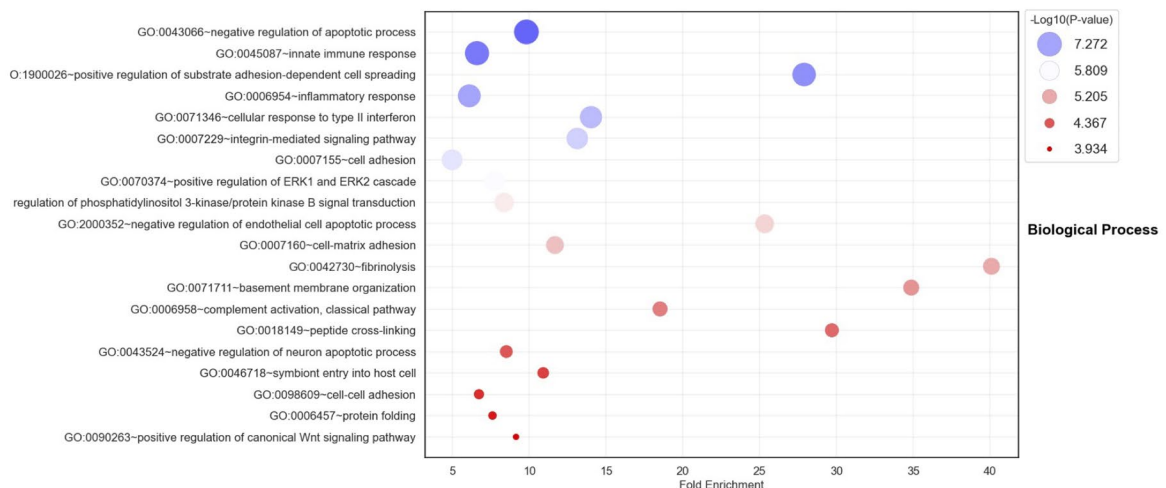


**Fig. 6** Proteomic comparison of naïveMSC-EVs and thMSC-EVs. **(A)** Bubble plot representation of top 30 Biological Processes enriched in thMSC-EVs than in naïve MSC-EVs. **(B)** Bubble plot representation of selected Biological Processes. Proteins that had more than two-fold greater abundance value in thMSC-EVs than in naïveMSC-EVs with  $p < 0.05$  were analyzed. Fisher's exact statistic was used to analyze protein enrichment. The size of the bubble represents protein counts

**Table 2** Representative proteins overexpressed in thMSC-EVs compared to the Naïve MSC-EVs

| Protein | FC (thEV/naiveEV) | GO term  |
|---------|-------------------|--|
| THBS1   | 10.38944103       | GO:0043066: negative regulation of apoptotic process   |
| TIMP1   | 11.94589969       | GO:0043066: negative regulation of apoptotic process   |
| ANXA1   | 3.773368868       | GO:0043066: negative regulation of apoptotic process<br>GO:0045087: innate immune response<br>GO:0098609: cell-cell adhesion |
| ITGB1   | 11.67722302       | GO:0098609: cell-cell adhesion   |
| FGF2    | 5.155911192       | GO:0090263: positive regulation of canonical Wnt signaling pathway   |

thMSC-EVs were enriched in these pathways and proteins exhibited more than two-fold increase in abundance. Detailed lists and fold change values can be found in the Supplementary Material 2. Among, the representative proteins under each pathway are listed in Table 2.

## Discussion

Herein, we primarily demonstrated that thMSC-EVs outperformed naïveMSC-EVs in enhancing cellular viability and integrity and reducing inflammation in established in vitro NEC models. Confirmed its enhanced therapeutic efficacy, thMSC-EVs were administered to the in vivo NEC model. In vivo, thMSC-EVs significantly reduced the macroscopic, histological, and biochemical markers of NEC injury, primarily through greater tissue preservation and reduced cell death. In NEC organoids, thMSC-EVs promoted ISC preservation and reduced stress-related marker levels, suggesting enhanced enterocyte maturation.

The mammalian intestinal epithelium regenerates every 4–5 days, driven by ISCs in the crypt base [42]. Effective NEC treatment in premature infants requires the reduction of tissue injury and the promotion of regeneration. Therefore, we comprehensively investigated the effects of thMSC-EVs in appropriate in vitro, in vivo, and organoid models.

In vitro NEC studies commonly stimulate the rat small intestinal cell line IEC-6 or the human colorectal adenocarcinoma cell line Caco-2 with LPS [43–46], which may be similar to the in vitro model of IBD [47]. To better mimic the in vivo induction of NEC, we concurrently induced hyperosmotic, ischemic, and hypothermic stress in IEC-6 cells and LPS in primary rat PMs. To improve the feasibility of the NEC protocol in vivo, we replaced overnight gavage feeding with overnight breastfeeding. This modification significantly reduced procedural risks

such as esophageal perforation, which improved survival rates while maintaining effective NEC induction and also reduced the investigator's burden. Although the breastmilk's benefits are well-known [48, 49], we confirmed that 60 µg of LPS, hyperosmolar formula, hypoxia, and hypothermia induced significant intestinal damage macroscopically, histologically, and biochemically. Furthermore, organoids derived from NEC-induced mouse pups have been established as alternative platforms for evaluating the therapeutic efficacy of thMSC-EVs.

In our in vitro model, thMSC-EVs showed significant anti-apoptotic, cellular integrity-enhancing, and anti-inflammatory effects on IEC-6 cells and PMs, whereas naïveMSC-EVs demonstrated milder effects. We previously confirmed that thrombin-preconditioned MSCs enrich their EVs with various growth factors such as vascular endothelial growth factor (VEGF) or brain-derived neuroprotective factors (BDNF) via Protease-activated receptor (PAR)-mediated signaling pathways [19, 22, 24]. However, to better understand thMSC-EVs' therapeutic effect in gastrointestinal injury, we analyzed the proteomics of naïveMSC-EVs and thMSC-EVs. Building on our previous observation of increased angiogenic cargo proteins in thMSC-EVs [22], our proteomic analysis notably revealed that key pathways critical for intestinal health, such as Wnt signaling, anti-apoptotic processes, cell adhesion, proliferation, and inflammatory responses, were also more than two-fold enriched in thMSC-EVs compared to naïveMSC-EVs. Though not validated in this study, we postulate that proteins presented in Table 2 may explain the in vitro results in enhanced cell survival, increased cellular integrity, and reduced inflammation. Under cell adhesion pathways, KRT18 and  $\alpha$ -catenin were noted which support cellular integrity and indirectly interact with ZO-1 [50–52]. Notably, Annexin-A1 (ANXA1) which is known to promote differentiation of monocytes into M2 phenotype [53] was three-fold enriched in thMSC-EVs, further explaining the significant increase in TGF- $\beta$  in thMSC-EVs treated LPS-induced peritoneal macrophages. Annexin-A1 plays a multi-faceted role, promoting anti-inflammation, pro-survival, and cell-cell adhesion, suggesting its possible role as a therapeutic component within thMSC-EVs, however further study must be done to confirm this. Enrichment of ERK1/2 pathway proteins, such as FGF2, that promote both epithelial and stem cell survival [54, 55], in thMSC-EVs support the improved cell survival of IEC-6 cells and increased ISC markers in vivo and in organoids. ZO-1 is a well-known tight junction protein under the occludins family, necessary for cell-cell adhesion and cellular integrity. When tight junctions are reduced, the intestinal epithelium becomes permeable, sequentially resulting in a leaky gut, microbial translocation into the body, and inflammation [56]. Both human

[57] and animal studies [58] have reported reduced tight junction proteins in NEC. Given the contribution of leaky epithelium to the NEC pathophysiology, evaluation of the ability to strengthen the intestinal barrier is critical in considering the NEC therapeutic. Therefore, our in vitro result presenting enhanced ability of thMSC-EVs in strengthening the integrity and proteomic results further support that thMSC-EVs are a promising therapeutic option for NEC. Future mechanistic studies using the proteomics data will provide a better understanding of thMSC-EVs' therapeutic effect.

Rodent models are advantageous in premature GI research because rodents are born underdeveloped, continuing maturation after birth, whereas full-term human neonates are fully developed before birth [59, 60]. The crypt-villi axis and the presence of mature enterocytes are evident in the human fetal intestine from 17 gestational weeks, which correlates with postnatal days 1–17 in neonatal mice [59–63]. At P7, mouse pups demonstrated well-defined crypt-villus morphology, diffuse *OLFM4*-positive ISCs at the crypt bottom, and the presence of mature goblet cells, enteroendocrine cells, and Paneth cell populations, suggesting that pups have developed small intestinal characteristics and cell populations (Supplemental Fig. 2B).

This study further confirmed that IP administration offers both gut-specific and systemic benefits, with thMSC-EVs localizing more to the NEC-induced small intestine than to the healthy intestine. The peritoneal cavity, rich in vascular and lymphatic networks [64], can serve as an alternative to the intravenous route when veins are technically inaccessible. By bypassing the pulmonary “first-pass” effect, IP administration allows systemic EV circulation, making it a preferable option for targeting the gut [65, 66], particularly in neonates with nil per os [6, 9]. Yet, confirmation of EVs' diffusion into lymphatic vessels must be explored. IP has been widely used to deliver MSCs in NEC models [11, 13, 14, 66, 67]. Herein, both systemic and local therapeutic effects of  $2 \times 10^9$  thMSC-EVs were indicated by significant improvements in clinical, histological, and biochemical evaluations, consistent with other reports in which MSCs were administered via IP in NEC models. For gut-specific effects, we postulated that diffused thMSC-EVs from the peritoneal cavity were closest to the crypt bottom, presenting anti-apoptotic and ISC-preserving effects. Future studies with longer observation periods will allow us to understand the downstream effects on mature enterocytes. Regarding systemic effects, the circulation of thMSC-EVs through the vasculature can be implied, which has also been observed in other studies using human bone marrow-MSCs ( $6 \times 10^5$  cells/50- $\mu$ L PBS) in a rat NEC model [11, 13]. Lastly, we suggest that thMSC-EVs exhibit a homing-like effect in MSCs,

in which significantly more cells are localized in NEC-induced intestines than in healthy controls [11, 13]. Although not motile like MSCs, thMSC-EVs were localized more in the injured gut than in the uninjured gut. Similar to a study tracking the migration of MSCs toward the NEC-induced gut [13], a future study tracking the diffusion of thMSC-EVs would better explain this phenomenon. Compared with MSCs, MSC-derived EVs, especially thMSC-EVs, offer distinct advantages as cell-free therapies with enhanced efficacy, increasing their potential as a therapeutic option.

Histological analysis confirmed that IP administration of  $2 \times 10^9$  thMSC-EVs reduced the extent of villus loss and cell death in LGR5- and *OLFM4*-positive intestinal stem cells. A greater number of goblet cells were observed, despite normalization with the number of villi present, implying that thMSC-EVs not only preserved more tissue but also supported the presence of more differentiated mature cell types, which are critical for mucosal barrier formation. A study previously compared the therapeutic efficacy of different stem cell sources ( $2 \times 10^6$  cells) [14] and their respective EVs ( $2.5 \times 10^9$ ) [21] in a rat NEC model. Similar to our study's integrity assessment, they used an FITC-labelled dextran permeability assay to confirm enhanced mucosal barrier function after stem cell administration [12, 20]. Although *Atoh1*, a marker of secretory precursor cells [68], showed a non-significant increase in expression following thMSC-EV treatment, the overall results suggest that thMSC-EVs promote intestinal regeneration.

ISC preservation is critical because ISCs drive the regeneration and differentiation of intestinal epithelial cells [69]. *OLFM4* and LGR5 are markers of adult ISCs that show increased expression throughout development and promote the differentiation of absorptive and secretory intestinal epithelial cells [70–72]. In this study, we confirmed increased adult ISC marker gene expression in the thMSC-EV-treated NEC+thEV group compared with that in the non-treated NEC group, both in vivo and in organoids. This may imply enhanced retention or protection of ISCs from intestinal damage, which is further supported by the co-localization of TUNEL-positive and *OLFM4*-positive cells. The increased *OLFM4* expression with age has been suggested as a hallmark of intestinal maturation by comparing human adult and fetal intestines [72, 73]. Upon intestinal damage, the loss of ISCs and reversion to a fetal-like state significantly reduces *OLFM4* expression in the intestine [74]. In organoids, a higher *OLFM4* expression level correlates with maturation and the ability to bud and differentiate into different lineages [75, 76]. Therefore, enhancing adult ISC function could be a key therapeutic goal in NEC treatment, as it facilitates the regeneration and maturation of the injured premature intestine. Significantly enriched proteins

under the Wnt signaling pathway, which is the main regulator of ISCs-mediated epithelial regeneration, further explain reduced villi loss and maintained ISC marker genes. Our persistent observation of enhanced cellular integrity can be similarly supported since Wnt signaling pathway is closely related to the cellular stability and integrity [77]. Our results suggest that thMSC-EVs may play a critical role in inducing the maturation or regeneration of premature and injured intestines by enhancing ISC gene expression levels via Wnt signaling pathway. Future studies will help further confirm the mechanism of the effect.

Since severe intestinal damage limits the evaluation of mature enterocytes, we differentiated organoids and treated them with thMSC-EVs to investigate their therapeutic effects on mature enterocytes. We observed that thMSC-EVs partly enhance the differentiation of organoids. This observation aligns with well-documented MSC's ability to regulate epithelial cell proliferation and differentiation [78]. In our proteomic analysis, thMSC-EVs were enriched with proteins under Notch and Wnt signaling pathways that promote intestinal stem cell maintenance and enterocyte differentiation [79, 80], which may have collectively contributed to enhanced differentiation of both CON and NEC organoids. Compared with untreated NEC organoids, we observed significantly reduced gene expression levels of *SI* and *CHGA*, which are stress-related markers, and *DEFA5*, which is an inflammatory marker, when treated with thMSC-EVs. *DEFA5*, an antimicrobial peptide [81, 82], is elevated in the inflamed human NEC intestine [81–83]. *SI* is a brush-border enzyme associated with the osmotic pressure regulation within the lumen, and its deficiency often results in NEC [84, 85]. *CHGA* plays a role in the chemosensing, hormone secretion, and motility of the GI tract [86], and although its role in NEC remains unclear, its elevated levels in patients with IBD suggest an association with inflammation [87–89]. The elevated expression of *SI*, *CHGA*, and *DEFA5* in NEC organoids compared with that in CON organoids was likely due to hyperosmotic stress and LPS exposure during *in vivo* induction. Reduced expression levels after 7 days of thMSC-EV treatment suggest the amelioration of GI stress, which will be better understood in future *in vivo* studies with longer observations of mature enterocytes. Overall, our results suggest that the injury memory persisted in the organoids through 3–4 passages and throughout differentiation and that thMSC-EVs ameliorated this effect.

One limitation of this study is the challenge of inducing substantial inflammation in an *in vivo* NEC model. A significant increase in IL- $\alpha$  levels in the NEC group compared with that in the CON group was observed; yet, changes in the levels of IL- $\beta$ , IL-6, and TNF- $\alpha$  were insignificant, despite significant intestinal damage confirmed

by histological and biochemical analysis (Supplemental Fig. 4). An increase in IL-1 $\alpha$  levels was reported in an NEC piglet model study [90]. A significant reduction in the elevated expression level of FABP6, an absorptive marker associated with inflammation in NEC, after thMSC-EV treatment was observed *in vivo* [39–41]. Many NEC animal studies primarily focused on histological damage rather than inflammation, despite inflammation being a key pathology in NEC. Conventional NEC mouse models, typically using C57BL/6J inbred strains, often differed only in the administration of LPS or cultured bacteria [17, 32, 43, 91–93]. Despite this, only a few studies presented inflammation by measuring MPO levels, an indication of neutrophil infiltration [13], and pro-inflammatory cytokines IL-6, IL-8, IL-1 $\beta$ , and TNF- $\alpha$  [43, 91] in NEC animal models, while many did not [11, 12, 14, 20, 21, 33]. To address this limitation, we treated IEC-6 cells *in vitro* with a primary rat PM CM to observe the effect of thMSC-EVs on PMs and subsequent damage to epithelial cells mimicking the *in vivo* status, and we observed a significant anti-inflammatory action of thMSC-EVs. In the future, a more refined experimental model might be needed to observe distinct time-dependent inflammatory changes mimicking clinical NEC.

In conclusion, this study confirmed the enhanced therapeutic effects of thMSC-EVs *in vitro*, including improved cell viability, strengthened cellular integrity, reduced pro-inflammatory cytokine secretion, and increased anti-inflammatory cytokine levels, compared with those of naïveMSC-EVs. We have further analyzed proteomic difference in the naïveMSC-EVs and thMSC-EVs to understand the therapeutic enhancement, and confirmed that cargo proteins were enriched in anti-apoptotic, anti-inflammatory, cell adhesion, Wnt signaling pathways. *In vivo*, we macroscopically confirmed the therapeutic effect of thMSC-EVs in improving clinical symptoms and increasing the GI length. thMSC-EVs preserved tissue, maintained the mucosal barrier, protected ISC populations, reduced cell death, and decreased IL-1 $\alpha$  levels. Biochemically, thMSC-EVs increased the expression of adult ISC markers and reduced the expression of FABP6. Organoid studies further confirmed that thMSC-EVs reduced inflammatory and injury responses while enhancing cellular integrity. Thus, thMSC-EVs are promising candidates for NEC therapy. Future studies should aim to investigate the clinically relevant time-point to administer thMSC-EVs and the mechanisms by which thMSC-EVs ameliorate intestinal injury, with extended observational periods, to further validate their therapeutic potential. To produce GMP-grade thMSC-EVs for clinical translation, it is essential to develop standardized production methods, cell banking with minimal batch variation, quality control, and cryopreserved formulations.

**Abbreviations**

|           |   |
|-----------|---|
| NEC       | Necrotizing Enterocolitis   |
| thMSC-EVs | Thrombin-preconditioned Mesenchymal Stromal Cell-derived Extracellular Vesicles |
| MSC       | Mesenchymal Stromal Cells   |
| EVs       | Extracellular Vesicles  |
| HIT       | Hyperosmotic, Ischemic, and Hypothermic   |
| IEC       | Intestinal Epithelial Cells   |
| LPS       | Lipopolysaccharide  |
| PMs       | Peritoneal Macrophages  |
| P4        | Postnatal Day 4   |
| IP        | Intraperitoneal   |
| NIHF      | Near-Infrared Fluorescence  |
| CON       | Control   |
| CM        | Conditioned Medium  |
| IL        | Interleukin   |
| TNF       | Tumor Necrosis Factor   |
| TGF       | Transforming Growth Factor  |
| OLFM4     | Olfactomedin 4  |
| CHGA      | Chromogranin A  |
| SI        | Sucrase-Isomaltase  |
| DEFA5     | Defensin 5  |
| CLDN4     | Claudin-4   |
| LC-MS/MS  | Liquid Chromatography with Tandem Mass Spectrometry                             |
| VEGF      | Vascular Endothelial Growth Factor  |
| BDNF      | Brain-Derived Neurotrophic Factor   |
| PAR       | Protease-Activated Receptor   |
| ERK       | Extracellular Signal-Regulated Kinase   |
| ANXA1     | Annexin A1  |
| WJ        | Wharton's Jelly   |
| FABP      | Fatty Acid-Binding Protein  |
| GAPDH     | Glyceraldehyde 3-Phosphate Dehydrogenase  |
| CCK-8     | Cell Counting Kit-8   |
| FITC      | Fluorescein Isothiocyanate  |
| PBS       | Phosphate Buffered Saline   |
| TUNEL     | TdT-mediated dUTP Nick-End Labeling   |
| DAPI      | 4',6-Diamidino-2-Phenylindole   |
| ELISA     | Enzyme-Linked Immunosorbent Assay   |
| RT-Qpcr   | Real-Time Quantitative Polymerase Chain Reaction                                |
| SAGE      | Serial Analysis of Gene Expression  |
| DAVID     | Database for Annotation, Visualization, and Integrated Discovery                |
| ARRIVE    | Animal Research: Reporting of In Vivo Experiments                               |
| IRB       | Institutional Review Board  |
| ICR       | Institute of Cancer Research  |

**Supplementary Information**

The online version contains supplementary material available at <https://doi.org/10.1186/s13287-025-04243-3>.

Supplementary Material 1  
 Supplementary Material 2  
 Supplementary Material 3  
 Supplementary Material 4  
 Supplementary Material 5  
 Supplementary Material 6  
 Supplementary Material 7  
 Supplementary Material 8

**Acknowledgements**

The authors declare that they have not used AI-generated work in this manuscript.

**Author contributions**

Conceptualization, Y.S.C., S.I.S.; Methodology & Formal analysis, S.H.; Investigation, S.H., S.I.S., Y.E.K., M.Y., A.K., S.Y.A., Y.S.C.; Writing-original draft: S.H., S.I.S.; Writing-review & editing, Y.S.C.; Funding acquisition: A.K., S.I.S., S.Y.A., Y.S.C.; Supervision, Y.S.C.

**Funding**

This research was supported by the Korean Fund for Regenerative Medicine (KFRM) grant funded by the Korean government Ministry of Science and ICT, the Ministry of Health & Welfare (22A0301L1); by a grant from Future Medicine 2030 Project from Samsung Medical Center (SMO1250011); by a grant from the Korea Health Technology R&D Project through the Korea Health Industry Development Institute (KHIDI), funded by the Ministry of Health & Welfare, Republic of Korea (KH129441); by the Korean Fund for Regenerative Medicine (KFRM) grant funded by the Korean government (Ministry of Science and ICT, Ministry of Health & Welfare) (23C0119L1); and by a grant of the Korea Health Technology R&D Project through the Korea Health Industry Development Institute (KHIDI), funded by the Ministry of Health & Welfare, Republic of Korea (RS-2024-00436750).

**Data availability**

All data generated or analyzed during this study are included in this published article and its supplementary information files.

**Declarations****Ethics approval and consent to participate**

Human WJ-MSCs from a single donor, which were collected with informed consent for the use of the study, were provided by the Samsung Medical Center Good Manufacturing Practice Facility (IRB approval number: 2016-07-102-043; Date of approval: 2016-09-20; Approval expiration date: 2025-09-15; Study name: Study on the Selection of Optimal Mesenchymal Stem Cells from Different Sources for the Treatment of Chronic/Intractable Diseases including Alzheimer's Disease and Musculoskeletal Disorders). All animal studies were reviewed and approved by the Institutional Animal Care and Use Committee (Approval numbers: 20231115001 and 20230116001. Approval Date: 2023.12.22 and 2023.02.22) of the Samsung Biomedical Research Institute, an Association for Assessment and Accreditation of Laboratory Animal Care-accredited facility, following the National Institutes of Health Guidelines for Laboratory Animal Care. Animal studies followed the ARRIVE guidelines.

**Consent for publication**

Not applicable.

**Conflict of interest**

The funders had no role in the study design; collection, analyses, or interpretation of data; writing of the manuscript; or decision to publish the results. Yun Sil Chang, Se In Sung, Young Eun Kim, Sein Hwang, and Ara Koh declare potential conflicts of interest arising from an issued patent titled "A composition for the prevention and treatment of necrotizing enterocolitis containing extracellular vesicles derived from thrombin-treated mesenchymal stem cells" (10-2024-0051684) as co-inventors, not as patentees.

**Author details**

<sup>1</sup>Department of Health Sciences and Technology, SAHST, Sungkyunkwan University, Seoul 06355, Republic of Korea

<sup>2</sup>Cell and Gene Therapy Institute for Future Medicine, Samsung Medical Center, Seoul 06351, Republic of Korea

<sup>3</sup>Department of Pediatrics, Samsung Medical Center, Sungkyunkwan University School of Medicine, Seoul 06351, Republic of Korea

<sup>4</sup>Department of Life Sciences, Pohang University of Science and Technology, Pohang 37673, South Korea

Received: 26 October 2024 / Accepted: 19 February 2025

Published online: 28 February 2025

**References**

1. Alsaied A, Islam N, Thalib L. Global incidence of necrotizing Enterocolitis: a systematic review and Meta-analysis. *BMC Pediatr.* 2020;20(1):344.

2. Fitzgibbons SC et al. *Mortality of necrotizing enterocolitis expressed by birth weight categories*. *J Pediatr Surg*. 2009; 44(6): pp. 1072-5; discussion 1075-6.
3. Yee WH, et al. Incidence and timing of presentation of necrotizing Enterocolitis in preterm infants. *Pediatrics*. 2012;129(2):e298–304.
4. Mekonnen SM, et al. The prevalence of necrotizing Enterocolitis and associated factors among enteral fed preterm and low birth weight neonates admitted in selected public hospitals in addis Ababa, Ethiopia: A Cross-sectional study. *Glob Pediatr Health*. 2021;8:2333794X211019695.
5. Patel BK, Shah JS. *Necrotizing enterocolitis in very low birth weight infants: a systemic review*. *ISRN Gastroenterol*, 2012. 2012: p. 562594.
6. Shulhan J, et al. Current knowledge of necrotizing Enterocolitis in preterm infants and the impact of different types of enteral nutrition products. *Adv Nutr*. 2017;8(1):80–91.
7. Jones IH, Hall NJ. Contemporary outcomes for infants with necrotizing Enterocolitis-A systematic review. *J Pediatr*. 2020;220:86–92. e3.
8. Nino DF, Sodhi CP, Hackam DJ. Necrotizing Enterocolitis: new insights into pathogenesis and mechanisms. *Nat Rev Gastroenterol Hepatol*. 2016;13(10):590–600.
9. Kasivajjula H, Maheshwari A. Pathophysiology and current management of necrotizing Enterocolitis. *Indian J Pediatr*. 2014;81(5):489–97.
10. Bazacliu C, Neu J. Necrotizing Enterocolitis: long term complications. *Curr Pediatr Rev*. 2019;15(2):115–24.
11. Tayman C, et al. Mesenchymal stem cell therapy in necrotizing Enterocolitis: a rat study. *Pediatr Res*. 2011;70(5):489–94.
12. Yang J, et al. Heparin-binding epidermal growth factor-like growth factor and mesenchymal stem cells act synergistically to prevent experimental necrotizing Enterocolitis. *J Am Coll Surg*. 2012;215(4):534–45.
13. Zani A, et al. Amniotic fluid stem cells improve survival and enhance repair of damaged intestine in necrotising Enterocolitis via a COX-2 dependent mechanism. *Gut*. 2014;63(2):300–9.
14. McCulloh CJ, et al. Stem cells and necrotizing Enterocolitis: A direct comparison of the efficacy of multiple types of stem cells. *J Pediatr Surg*. 2017;52(6):999–1005.
15. McCulloh CJ, et al. Evaluating the efficacy of different types of stem cells in preserving gut barrier function in necrotizing Enterocolitis. *J Surg Res*. 2017;214:278–85.
16. Weis VG, et al. Human placental-derived stem cell therapy ameliorates experimental necrotizing Enterocolitis. *Am J Physiol Gastrointest Liver Physiol*. 2021;320(4):G658–74.
17. Li B, et al. Intestinal epithelial tight junctions and permeability can be rescued through the regulation of Endoplasmic reticulum stress by amniotic fluid stem cells during necrotizing Enterocolitis. *FASEB J*. 2021;35(1):e21265.
18. Baek G, et al. Mesenchymal stem Cell-Derived extracellular vesicles as therapeutics and as a drug delivery platform. *Stem Cells Transl Med*. 2019;8(9):880–6.
19. Sung DK et al. Thrombin preconditioning of extracellular vesicles derived from mesenchymal stem cells accelerates cutaneous wound healing by boosting their biogenesis and enriching cargo content. *J Clin Med*, 2019. 8(4).
20. Rager TM, et al. Exosomes secreted from bone marrow-derived mesenchymal stem cells protect the intestines from experimental necrotizing Enterocolitis. *J Pediatr Surg*. 2016;51(6):942–7.
21. McCulloh CJ, et al. Treatment of experimental necrotizing Enterocolitis with stem cell-derived exosomes. *J Pediatr Surg*. 2018;53(6):1215–20.
22. Sung DK et al. Thrombin preconditioning boosts biogenesis of extracellular vesicles from mesenchymal stem cells and enriches their cargo contents via Protease-Activated Receptor-Mediated signaling pathways. *Int J Mol Sci*, 2019. 20(12).
23. Kim YE et al. Thrombin Preconditioning Enhances Therapeutic Efficacy of Human Wharton's Jelly-Derived Mesenchymal Stem Cells in Severe Neonatal Hypoxic Ischemic Encephalopathy. *Int J Mol Sci*, 2019. 20(10).
24. Jung SY et al. Thrombin preconditioning improves the therapeutic efficacy of mesenchymal stem cells in severe intraventricular hemorrhage induced neonatal rats. *Int J Mol Sci*, 2022. 23(8).
25. Ahn SY, et al. Brain-derived neurotrophic factor mediates neuroprotection of mesenchymal stem cell-derived extracellular vesicles against severe intraventricular hemorrhage in newborn rats. *Stem Cells Transl Med*. 2021;10(3):374–84.
26. Kim YE et al. Mesenchymal-Stem-Cell-Derived extracellular vesicles attenuate brain injury in *Escherichia coli* meningitis in newborn rats. *Life (Basel)*, 2022. 12(7).
27. Bang Y, et al. Therapeutic efficacy of thrombin-preconditioned mesenchymal stromal cell-derived extracellular vesicles on *Escherichia coli*-induced acute lung injury in mice. *Respir Res*. 2024;25(1):303.
28. Tanner SM, et al. Pathogenesis of necrotizing Enterocolitis: modeling the innate immune response. *Am J Pathol*. 2015;185(1):4–16.
29. Schwartz L, et al. Hyperosmotic stress contributes to mouse colonic inflammation through the methylation of protein phosphatase 2A. *Am J Physiol Gastrointest Liver Physiol*. 2008;295(5):G934–41.
30. Brocker C, Thompson DC, Vasilou V. The role of hyperosmotic stress in inflammation and disease. *Biomol Concepts*. 2012;3(4):345–64.
31. Neuhofer W. Role of NFAT5 in inflammatory disorders associated with osmotic stress. *Curr Genomics*. 2010;11(8):584–90.
32. Nolan LS, et al. A protocol for the induction of experimental necrotizing Enterocolitis in neonatal mice. *STAR Protoc*. 2021;2(4):100951.
33. Zani A, et al. Assessment of a neonatal rat model of necrotizing Enterocolitis. *Eur J Pediatr Surg*. 2008;18(6):423–6.
34. Jilling T, et al. The roles of bacteria and TLR4 in rat and murine models of necrotizing Enterocolitis. *J Immunol*. 2006;177(5):3273–82.
35. Sato T, et al. Long-term expansion of epithelial organoids from human colon, adenoma, adenocarcinoma, and Barrett's epithelium. *Gastroenterology*. 2011;141(5):1762–72.
36. Garg PM, et al. Clinical determinants and impact of hemorrhagic lesions on intestinal pathology in preterm infants with surgical necrotizing Enterocolitis. *J Neonatal Perinat Med*. 2023;16(1):119–28.
37. Elmore SA, et al. Recommendations for the INHAND apoptosis/necrosis working group. *Toxicol Pathol*. 2016;44(2):173–88.
38. César Machado MC, et al. Circulating fatty acid binding protein as a marker of intestinal failure in septic patients. *Crit Care*. 2012;16(6):455.
39. Schurink M, et al. Intestinal fatty Acid-Binding protein as a diagnostic marker for complicated and uncomplicated necrotizing Enterocolitis: A prospective cohort study. *PLoS ONE*. 2015;10(3):e0121336.
40. Pelsers MM, et al. Intestinal-type and liver-type fatty acid-binding protein in the intestine. Tissue distribution and clinical utility. *Clin Biochem*. 2003;36(7):529–35.
41. Guthmann F, et al. Plasma concentration of intestinal- and liver-FABP in neonates suffering from necrotizing Enterocolitis and in healthy preterm neonates. *Mol Cell Biochem*. 2002;239(1–2):227–34.
42. van der Flier LG, Clevers H. Stem cells, self-renewal, and differentiation in the intestinal epithelium. *Annu Rev Physiol*. 2009;71:241–60.
43. Sodhi CP, et al. The human milk oligosaccharides 2'-fucosyllactose and 6'-sialyllactose protect against the development of necrotizing Enterocolitis by inhibiting toll-like receptor 4 signaling. *Pediatr Res*. 2021;89(1):91–101.
44. De Fazio L et al. Necrotizing Enterocolitis: overview on in vitro models. *Int J Mol Sci*, 2021. 22(13).
45. Lyu C, et al. Vitamin D protects against necrotising Enterocolitis in newborn mice by activating the ERK signalling pathway. *Mol Med Rep*. 2020;22(3):2107–14.
46. Ares G, et al. Caveolin 1 is associated with upregulated Claudin 2 in necrotizing Enterocolitis. *Sci Rep*. 2019;9(1):4982.
47. Joshi A, Soni A, Acharya S. Vitro models and ex vivo systems used in inflammatory bowel disease. *Vitro Model*. 2022;1(3):213–27.
48. Herrmann K, Carroll K. An exclusively human milk diet reduces necrotizing Enterocolitis. *Breastfeed Med*. 2014;9(4):184–90.
49. Altobelli E et al. The impact of human milk on necrotizing Enterocolitis: A systematic review and Meta-Analysis. *Nutrients*, 2020. 12(5).
50. Drees F, et al. Alpha-catenin is a molecular switch that binds E-cadherin-beta-catenin and regulates actin-filament assembly. *Cell*. 2005;123(5):903–15.
51. Muller SL, et al. The tight junction protein occludin and the adherens junction protein alpha-catenin share a common interaction mechanism with ZO-1. *J Biol Chem*. 2005;280(5):3747–56.
52. Coulombe PA, Omary MB. Hard' and 'soft' principles defining the structure, function and regulation of keratin intermediate filaments. *Curr Opin Cell Biol*. 2002;14(1):110–22.
53. Yan Z, et al. Therapeutic potential for targeting Annexin A1 in fibrotic diseases. *Genes Dis*. 2022;9(6):1493–505.
54. Balmanno K, Cook SJ. Tumour cell survival signalling by the ERK1/2 pathway. *Cell Death Differ*. 2009;16(3):368–77.
55. Houchen CW, et al. FGF-2 enhances intestinal stem cell survival and its expression is induced after radiation injury. *Am J Physiol*. 1999;276(1):G249–58.
56. Horowitz A, et al. Paracellular permeability and tight junction regulation in gut health and disease. *Nat Rev Gastroenterol Hepatol*. 2023;20(7):417–32.

57. Bein A, et al. Intestinal tight junctions are severely altered in NEC preterm neonates. *Pediatr Neonatol*. 2018;59(5):464–73.
58. Ravisankar S, et al. Necrotizing Enterocolitis leads to disruption of tight junctions and increase in gut permeability in a mouse model. *BMC Pediatr*. 2018;18(1):372.
59. Stanford AH, et al. A direct comparison of mouse and human intestinal development using epithelial gene expression patterns. *Pediatr Res*. 2020;88(1):66–76.
60. Dehmer JJ, et al. Expansion of intestinal epithelial stem cells during murine development. *PLoS ONE*. 2011;6(11):e27070.
61. Kwon O, Han TS, Son MY. Intestinal morphogenesis in development, regeneration, and disease: the potential utility of intestinal organoids for studying compartmentalization of the Crypt-Villus structure. *Front Cell Dev Biol*. 2020;8:593969.
62. Trier JS, Moxey PC. Morphogenesis of the small intestine during fetal development. *Ciba Found Symp*. 1979;70:3–29.
63. Fawcner-Corbett D, et al. Spatiotemporal analysis of human intestinal development at single-cell resolution. *Cell*. 2021;184(3):810–e82623.
64. Olin T, Saldeen T. The lymphatic pathways from the peritoneal cavity: A lymphangiographic study in the rat. *Cancer Res*. 1964;24:1700–11.
65. Wang M, et al. Intraperitoneal injection (IP), intravenous injection (IV) or anal injection (AI)? Best way for mesenchymal stem cells transplantation for colitis. *Sci Rep*. 2016;6:30696.
66. Ghionzoli M, et al. Amniotic fluid stem cell migration after intraperitoneal injection in pup rats: implication for therapy. *Pediatr Surg Int*. 2010;26(1):79–84.
67. Al Shoyaib A, Archie SR, Karamyan VT. Intraperitoneal route of drug administration: should it be used in experimental animal studies?? *Pharm Res*. 2019;37(1):12.
68. Ishibashi F, et al. Contribution of ATOH1(+) cells to the homeostasis, repair, and tumorigenesis of the colonic epithelium. *Stem Cell Rep*. 2018;10(1):27–42.
69. Venkatraman A et al. Intestinal stem cell development in the neonatal Gut: pathways regulating development and relevance to necrotizing Enterocolitis. *Cells*, 2021. 10(2).
70. van der Flier LG, et al. OLFM4 is a robust marker for stem cells in human intestine and marks a subset of colorectal cancer cells. *Gastroenterology*. 2009;137(1):15–7.
71. VanDussen KL, et al. Notch signaling modulates proliferation and differentiation of intestinal crypt base columnar stem cells. *Development*. 2012;139(3):488–97.
72. Tsai YH, et al. Acquisition of NOTCH dependence is a hallmark of human intestinal stem cell maturation. *Stem Cell Rep*. 2022;17(5):1138–53.
73. Finkbeiner SR, et al. Transcriptome-wide analysis reveals hallmarks of human intestine development and maturation in vitro and in vivo. *Stem Cell Rep*. 2015;4(6):1140–55.
74. Nusse YM, et al. Parasitic helminths induce fetal-like reversion in the intestinal stem cell niche. *Nature*. 2018;559(7712):109–13.
75. Sprangers J, Zaalberg IC, Maurice MM. Organoid-based modeling of intestinal development, regeneration, and repair. Volume 28. *Cell Death & Differentiation*; 2021. pp. 95–107. 1.
76. Fordham RP, et al. Transplantation of expanded fetal intestinal progenitors contributes to colon regeneration after injury. *Cell Stem Cell*. 2013;13(6):734–44.
77. Amin N, Vincan E. The Wnt signaling pathways and cell adhesion. *Front Biosci (Landmark Ed)*. 2012;17(2):784–804.
78. Gong W, et al. Mesenchymal stem cells stimulate intestinal stem cells to repair radiation-induced intestinal injury. *Cell Death Dis*. 2016;7(9):e2387.
79. Fevr T, et al. Wnt/beta-catenin is essential for intestinal homeostasis and maintenance of intestinal stem cells. *Mol Cell Biol*. 2007;27(21):7551–9.
80. Carulli AJ, et al. Notch receptor regulation of intestinal stem cell homeostasis and crypt regeneration. *Dev Biol*. 2015;402(1):98–108.
81. Salzman NH, Underwood MA, Bevins CL. Paneth cells, defensins, and the commensal microbiota: a hypothesis on intimate interplay at the intestinal mucosa. *Semin Immunol*. 2007;19(2):70–83.
82. Ayabe T, et al. Secretion of microbicidal alpha-defensins by intestinal Paneth cells in response to bacteria. *Nat Immunol*. 2000;1(2):113–8.
83. Salzman NH, et al. Enteric defensin expression in necrotizing Enterocolitis. *Pediatr Res*. 1998;44(1):20–6.
84. Gericke B, Amiri M, Naim HY. The multiple roles of sucrase-isomaltase in the intestinal physiology. *Mol Cell Pediatr*. 2016;3(1):2.
85. Thymann T, et al. Carbohydrate maldigestion induces necrotizing Enterocolitis in preterm pigs. *Am J Physiol Gastrointest Liver Physiol*. 2009;297(6):G1115–25.
86. Latorre R, et al. Enteroendocrine cells: a review of their role in brain-gut communication. *Neurogastroenterol Motil*. 2016;28(5):620–30.
87. Massironi S, et al. Chromogranin A and other enteroendocrine markers in inflammatory bowel disease. *Neuropeptides*. 2016;58:127–34.
88. Mazzawi T, El-Salhy M. Changes in small intestinal chromogranin A-immunoreactive cell densities in patients with irritable bowel syndrome after receiving dietary guidance. *Int J Mol Med*. 2016;37(5):1247–53.
89. Sciola V, et al. Plasma chromogranin a in patients with inflammatory bowel disease. *Inflamm Bowel Dis*. 2009;15(6):867–71.
90. Cho SX, et al. The immunological landscape in necrotising Enterocolitis. *Expert Rev Mol Med*. 2016;18:e12.
91. Wang C, et al. Human milk oligosaccharides protect against necrotizing Enterocolitis by inhibiting intestinal damage via increasing the proliferation of crypt cells. *Mol Nutr Food Res*. 2019;63(18):e1900262.
92. Klinke M, et al. Development of an improved murine model of necrotizing Enterocolitis shows the importance of neutrophils in NEC pathogenesis. *Sci Rep*. 2020;10(1):8049.
93. O'Connell JS, et al. Treatment of necrotizing Enterocolitis by conditioned medium derived from human amniotic fluid stem cells. *PLoS ONE*. 2021;16(12):e0260522.

## Publisher's note

Springer Nature remains neutral with regard to jurisdictional claims in published maps and institutional affiliations.